Mitochondrial H_2S donor AP39 induces stomatal closure by modulating guard cell mitochondrial activity

Rosario Pantaleno[1], Denise Scuffi[1], Alex Costa[2], Elina Welchen[3], Roberta Torregrossa[4], Matthew Whiteman[4], Carlos García-Mata[1]

[1]Instituto de Investigaciones Biológicas, Universidad Nacional de Mar del Plata, Consejo Nacional de Investigaciones Científicas y Técnicas, 7600 Mar del Plata, Argentina.

[2]University of Milan, Department of Biosciences, Milan, 20133, Italy

[3]Instituto de Agrobiotecnología del Litoral (CONICET-UNL). Cátedra de Biología Celular y Molecular, Facultad de Bioquímica y Ciencias Biológicas, Universidad Nacional del Litoral, 3000 Santa Fe, Argentina.

[4]University of Exeter Medical School, St. Luke's Campus, Exeter EX1 2LU, UK

***Corresponding author**:

Carlos García-Mata

e-mail: camata@mdp.edu.ar

The author responsible for distribution of materials integral to the findings presented in this article in accordance with the policy described in the Instructions for Authors (https://academic.oup.com/plphys/pages/General-Instructions) is Carlos García-Mata.

Author contributions:

RP performed most of the experiments, analysed the data and wrote the article, DS performed experiments from Figure 1, analysed the data and helped with the writing of the article, RT and MW contributed with the reagents and assisted in the writing of the article, EW provided biological material and contributed to discussion, AC participated in the experimental design and discussion, and CGM conceived the project, analysed the data wrote the article.

Short title: Mitochondrial H_2S induces stomatal closure

ABSTRACT

Hydrogen sulfide (H_2S) is a gaseous signaling molecule involved in numerous physiological processes in plants, including gas exchange with the environment through the regulation of stomatal pore width. Guard cells are pairs of specialized epidermal cells that delimit stomatal pores and have a higher mitochondrial density and metabolic activity than their neighboring cells. However, there is no clear evidence on the role of mitochondrial activity in stomatal closure induction. In this work, we showed that the mitochondrial-targeted H_2S donor AP39 induces stomatal closure in a dose-dependent manner. Experiments using inhibitors of the mitochondrial electron transport chain (mETC) or insertional mutants in cytochrome *c* (CYTc) indicated that the activity of mitochondrial CYTc and/or complex IV are required for AP39-dependent stomatal closure. By using fluorescent probes and genetically-encoded biosensors we reported that AP39 hyperpolarized the mitochondrial inner potential ($\Delta\psi m$) and increased cytosolic ATP, cytosolic hydrogen peroxide levels, and oxidation of the glutathione pool in guard cells. These findings showed that mitochondrial-targeted H_2S donors induce stomatal closure, modulate guard cell mitochondrial ETC activity, the cytosolic energetic and oxidative status, pointing to an interplay between mitochondrial H_2S, mitochondrial activity, and stomatal closure.

INTRODUCTION

Most land plants have microscopic structures in the epidermal layer of leaves called stomata, consisting of a central pore surrounded by pairs of highly specialized cells, known as guard cells (GCs). Stomata are responsible for the gas exchange between the plant and the environment, controlling O_2 release to the atmosphere, CO_2 uptake needed for photosynthesis, and water loss through the transpiration stream (Lawson and Matthews, 2020). This trade-off between CO_2 uptake for photosynthesis, and the loss of water, is tightly controlled through the regulation of the stomatal pore width. This is possible due to the ability of guard cells to perceive internal and external stimuli, which are then integrated and transduced via a complex signaling network (Hetherington & Woodward, 2003).

Guard cells have unique characteristics that distinguish them from their neighboring cells, including the presence of fewer and smaller chloroplasts (Wille and Lucas, 1984), a higher

mitochondrial density (Willmer and Fricker, 1996) and respiratory rate (Araújo et al., 2011). These features point towards a key function of mitochondria in GC's physiological processes, and as a consequence, on stomatal movement regulation. The requirement of sucrose, starch and triacylglycerol breakdown during light-induced stomatal opening (Daloso et al., 2015; Horrer et al., 2016; McLachlan et al., 2016) highlights the role of mitochondrial metabolism in this response. In addition, it was recently shown that GC's mitochondria are the main source of cytosolic ATP, needed for stomatal opening (Lim et al., 2022). However, the role of mitochondrial activity during stomatal closure remains unexplored.

Hydrogen sulfide (H_2S) is a low-weight gas endogenously synthesized in cells. It can freely diffuse across biological membranes and is considered very reactive at physiological pH and temperature conditions (Benchoam et al., 2019). H_2S is the third member of the so-called "gasotransmitters" group (García-Mata and Lamattina, 2013), which also includes nitric oxide (NO) and carbon monoxide (CO). All of them share similar chemical properties and are considered relevant signaling molecules in organisms from different kingdoms (Aroca et al., 2020) .

H_2S participates in diverse cellular processes throughout plant's life cycle, such as germination (Baudouin et al., 2016), autophagy (Laureano-Marín et al., 2020), and stomatal closure regulation (García-Mata and Lamattina, 2010; Lisjak et al., 2010), among others. The biosynthesis of H_2S occurs in different sub-cellular compartments including the cytosol, chloroplast, and mitochondria. Although H_2S can participate in different types of reactions, latest reports suggest that its biological role is exerted trough persulfidation, an oxidative posttranslational modification in cysteine residues (Filipovic et al., 2018).

In animal experimental systems, mitochondrial H_2S (mt-H_2S) is reported to exert cytoprotective effects via the modulation of cellular ATP levels, as well as stimulating/preserving cellular bioenergetics (Szabo et al., 2014; Fox et al., 2021). The normal electron flow through the mitochondrial electron transport chain (mETC) is coupled to proton pumping, generating an electrical potential ($\Delta\psi m$) between both sides of the inner membrane, which is the driving force required for mitochondrial ATP synthesis by the ATP synthase complex (Braun, 2020). In prokaryotes and many metazoans including invertebrates, fish, birds, and mammals, H_2S can donate electrons to the mETC (Olson and Straub, 2016). Moreover, in human cell cultures, H_2S persulfidates the mitochondrial ATP synthase, increasing its activity (Módis et

al., 2016); while the reduction of cytochrome *c* (CYTc), promotes O_2 consumption (Vitvitsky et al., 2018). The use of mitochondrial-targeted H_2S donors in animal systems has shown that H_2S is able to restore membrane polarization, helping to preserve mitochondrial function (Ie Trionnaire et al., 2014; Fox et al., 2021).

On the other hand, despite advances in the knowledge of the mitochondrial H_2S enzymatic source in Arabidopsis (*Arabidopsis thaliana*) (García et al., 2010), little is known about the effect of mt-H_2S in plants. In this work, we studied the role of mt-H_2S in GCs employing H_2S donors targeted specifically to mitochondria. Results show that mt-H_2S participates in stomatal closure induction through the modulation of mitochondrial activity in GCs.

RESULTS

Mitochondrial H_2S donors induce stomatal closure

Given the lack of information on the use of mitochondrial targeted H_2S in plants, as a first approach, we performed a dose-response assay in order to address whether mitochondrial H_2S has any effect on stomatal movement. With that aim, we treated *Arabidopsis thaliana* epidermal peels (strips) with increasing concentrations of the mt-H_2S donor AP39. Epidermal strips were incubated for 3 hours in opening buffer (OB: 5 mM MES, 50 mM KCl, pH=6.1) under white light, to open the stomatal pores, and then the strips were treated for 90 min, in the same OB, with increasing concentrations of AP39 (Fig. 1A). The addition of the mt-H_2S donor induced stomatal closure in a dose-dependent manner yielding a maximum effect, 30% reduction of the stomatal pore width, at a concentration of 0.1-1 µM AP39. As 100 nM was the minimal dose with the maximum effect, we selected it as the working concentration for the following assays (3.32±0.84 µm and 2.35±0.65 µm for mock and 100 nM AP39, respectively). Interestingly, the treatment with the master regulator of stomatal closure, abscisic acid (ABA), is reported to induce the same percentage of response (Scuffi et al., 2014). In addition, treating the epidermal strips with 100 µM of the widely used general H_2S donor GYY4137 yielded a stomatal closure range comparable to that obtained with a concentration of AP39 2-3 orders of magnitude lower. To test if the mitochondrial donor was affecting GC viability, Arabidopsis epidermal strips were

placed in OB and treated with 0.001 to 10 µM AP39 for 90 min, and then loaded with the viability fluorescent dye, Fluorescein diacetate (FDA). GC viability was quantified as the ratio between fluorescent GCs over total GCs. As observed in Fig. 1B, the exposure to mt-H_2S only compromised GC viability at the higher concentration assayed (10 µM), where the stomatal closure induction was suboptimal, discarding the possibility of a toxic effect of the donor molecule on stomata.

In addition, we treated Arabidopsis peels with AP39 in the presence of the H_2S scavenger hypotaurine (HT), or with two other mitochondrial-targeted H_2S donors, AP123 and RT01 (Fig. 1C, Supplemental Fig. 1A,B). The fact that HT impaired AP39-induced stomatal closure, and that both AP123 and RT01 showed a dose-dependent response comparable to that observed for AP39, indicate that stomatal closure was triggered by mitochondrial H_2S. Finally, the same AP39 concentrations used for Arabidopsis stomatal closure assays were added to fava bean (*Vicia faba*) epidermal strips. As observed in Supplemental Fig. S1C, Vicia epidermal strips also showed a dose-dependent stomatal response, indicating that the AP39 effect was not dependent on the plant species.

Mitochondrial ETC complex IV and/or cytochrome C activity are required for AP39 dependent stomatal closure

In human cellular cultures, mt-H_2S donors were shown to modulate mitochondrial function through the interaction with different members of the mETC (Módis et al., 2016; Vitvitsky et al., 2018). Therefore, we sought to test whether GC mitochondrial activity is involved in mt-H_2S-dependent stomatal closure induction. Following that purpose, Arabidopsis epidermal strips were treated with AP39, with or without the addition of the mETC inhibitors Rotenone (Rtn), 2-Thenoyltrifluoroacetone (TTFA), Antimycin A (AA) or Potassium cyanide (KCN) (inhibitors of the mETC complexes I, II, III and IV, respectively) (Fig. 2A). Stomatal pore width measurements showed that the exposure to the inhibitors of mETC complexes I to III had no effect on AP39-dependent stomatal closure, inducing a reduction of the stomatal pore size comparable to that obtained with AP39 alone (3.51±1.42 µm – 3.36±1.19 µm, 3.26±1.07 µm – 3.39±1.12 µm, 3.26±1.07 µm – 3.24±1 µm for AP39 alone or in the presence of Rtn, TTFA or AA, respectively) (Fig. 2B-D). Interestingly, the addition of KCN impaired AP39-induced stomatal closure (2.78±1.02 µm and 3.37±1.08 µm for AP39 and KCN + AP39, respectively), suggesting that

an active mETC complex IV is needed for mt-H_2S-dependent stomatal closure (Fig. 2E). To rule out a putative toxic effect of KCN on GCs, we treated epidermal strips with other widely-used stomatal closure stimuli in the presence or absence of KCN. Supplemental Figure S2 shows that induction of stomatal closure by ABA (but not by darkness) was partially inhibited by KCN (Mock=4.07±1.12 µm, ABA=2.78±0.9 µm, KCN+ABA=3.44±1.09 µm (A); Mock=3.99±1.14 µm, darkness=3.09±0.94 µm, KCN + darkness=3.29±0.96 µm (B)). In addition, KCN treatments performed in FDA-loaded epidermal strips, showed that the fluorescence levels were not affected upon 2h of KCN treatment, indicating that stomatal viability was not compromised by the addition of KCN (Supplemental Fig. S2C).

To further test the requirement of a functional mETC for AP39-triggered stomatal closure, we assessed the stomatal response in plants with a mutated Cytochrome c (CYTc). CYTc is an heme protein located in the intermembrane space (IMS) that functions as an electron carrier between complexes III and IV (Welchen and Gonzalez, 2016). *Arabidopsis thaliana* has two genes coding for CYTc: *CYTC-1* and *CYTC-2*. In addition to its role as an electron carrier, CYTc is also required for complex IV stability, whose activity and amount is dependent on CYTc levels (Welchen et al., 2012). We measured the stomatal response to AP39 in single and double *CYTc* Arabidopsis mutants. The lines *1*a and *1*b are insertional mutants in the gene *CYTC-1*, while *2*a and *2*b contain insertions in the gene *CYTC-2* (Welchen et al., 2012). Results in Figure 3 show that in the single mutants, AP39 induces stomatal closure comparable to that observed in WT plants, however, the stomatal response is impaired in the double mutants, indicating that CYTc is involved in AP39 response. The differences between the single and the double mutants' response is in agreement with previous results that reported the existence of a functional redundancy between both CYTc (Welchen et al., 2012). Moreover, we observed that ABA treatment induced stomatal closure in double mutants (Supplemental Fig. S3), showing that CYTc activity is needed particularly for mt-H_2S signaling pathway.

AP39 hyperpolarizes mitochondrial membrane potential in GCs

The requirement of normal CYTc/complex IV activity for AP39-dependent stomatal closure prompted us to analyse the effect of AP39 on mitochondrial inner membrane potential (Δψm) as an indicator of mETC activity (Zorova et al., 2018). For this purpose, Arabidopsis epidermal strips, expressing a mitochondrial-targeted GFP (mito-GFP) (Logan and Leaver, 2000), were loaded with the fluorescent probe red tetramethylrhodamine, methyl ester (TMRM), which accumulates, reversibly, in the mitochondrial matrix depending on the polarization state of the inner membrane (Brand and Nicholls, 2011). TMRM fluorescence intensity increases upon mitochondrial membrane hyperpolarization and decreases when the mitochondrial membrane is less polarized, while GFP intensity is not dependent on the variation of mitochondrial membrane potential. Mito-GFP epidermal strips were pre-incubated in the dark in OB supplemented with TMRM and then treated with DMSO 0.01% (Mock) or AP39. The ratio between TMRM and GFP fluorescence intensity was calculated for each GC (Fig. 4). AP39 increased the TMRM/GFP ratio on GCs (Fig. 4B), and hence the GCs Δψm, suggesting a mt-H_2S-dependent increase on mETC activity. In order to measure another indicator of mitochondria activity, we studied the effect of AP39 on GCs cytosolic ATP pool.

AP39 increases ATP levels in GCs

We used Arabidopsis plants expressing the genetically encoded FRET-based sensor ATeam1.03-nD/na, which contains a ε-subunit fragment of ATP synthase from Bacillus sp. PS3, and two fluorophores, a monomeric super-enhanced cyan fluorescent protein (mseCFP) and a circularly permuted monomeric Venus (cp173-mVenus) (Imamura et al., 2009; Kotera et al., 2010)). ATeam1.03-nD/Na recognizes $MgATP^{-2}$, the biologically relevant portion of ATP pool, and the interaction leads to a conformational modification of the protein, increasing the FRET efficiency. The simultaneous detection of both fluorescence emissions and the calculation of the Venus/CFP ratio of GCs, provides a dynamic readout of the $MgATP^{-2}$ levels in cytosol.

Arabidopsis epidermal strips expressing ATeam1.03-nD/na were placed in OB for at least 60 min in the dark, to avoid the effects of active photosynthesis (de Col et al., 2017), and then treated or not with AP39. The Venus/CFP ratio calculated for each GC shows that AP39 increased

the cytosolic $MgATP^{-2}$ levels, compared with steady conditions (Fig. 5), providing further evidence on the effect of mt-H_2S on the modulation of mitochondrial bioenergetics.

AP39 increases H_2O_2 levels and the oxidation of glutathione in the cytosol

In different animal experimental systems, AP39 was shown to exert its effect not only through the modulation of mitochondrial activity, but also through the regulation of intracellular signaling components, among them, reactive oxygen species (ROS) (Covarrubias et al., 2019). In plants, there is no information of mt-H_2S regulation, but we reported the existence of an interplay between H_2S and H_2O_2 during stomatal closure induction. To study whether mt-H_2S has any effect on ROS modulation and/or the cellular redox state, we measured cytosolic H_2O_2 levels and the glutathione (GSH) oxidation status in GCs treated with AP39. In order to detect *in vivo* and reversibly the H_2O_2 and the GSH/GSSH ratio dynamics in GCs, we employed Arabidopsis plants expressing the fluorescent proteins roGFP2-Orp1 and Grx1-roGFP2 (Scuffi et al., 2018; Nietzel et al., 2019), respectively. The sensor roGFP2-Orp1 is a construct that contains the yeast peroxidase Orp1 fused to redox sensitive ro-GFP2, while Grx1-roGFP2 has ro-GFP2 fused to human glutaredoxin (Grx1) (Gutscher et al., 2009; Nietzel et al., 2019). Epidermal strips from roGFP2-Orp1 and Grx1-roGFP2 plants were treated or not with AP39 at different times, according to Scuffi *et al.*, 2018. Figure 6 shows that AP39 induced the oxidation of both biosensors in GCs (Fig. 6A,B), indicating that mt-H_2S increases the H_2O_2 content and the oxidation of the GSH. Furthermore, when strips were treated with AP39 in presence of HT, there was no evident increase on the oxidation of roGFP2-Orp1 (Fig. 6C) supporting the involvement of H_2S in this response.

DISCUSSION

H_2S is already established as a signaling molecule with physiological roles in organisms from the five kingdoms (Olson and Straub, 2016; Aroca et al., 2020). The main enzymatic source of H_2S in animal systems, Cystathionine γ-lyase (CSE), is localized in the cytosol, however, under certain stress conditions it can translocate to the mitochondria and exert different physiological roles through mt-H_2S production (Fu et

al., 2012). On the other hand, the role of the endogenously synthesized mt-H_2S in plants remains unclear because most of the knowledge about the biological function of H_2S comes from pharmacological data, using the general H_2S donors NaHS and GYY4137, or from genetic data related to the cytosolic source DES1 (Scuffi et al., 2018; Shen et al., 2020).

In the present study we prove that mt-H_2S, released by mitochondrial-targeted H_2S delivery molecules, induces stomatal closure in a CYTc and/or complex IV dependent manner (Fig. 2 and Fig. 3). The suboptimal response at the higher concentration assayed, corresponds with a reduction in guard cell viability (Fig. 1B), which resembles the biphasic dose-response observed for mt-H_2S in animal's mitochondria (Szabo et al., 2014). In the latter, high concentrations of mt-H_2S inhibit mitochondrial activity, an effect associated to mitochondrial-derived diseases (Panagaki et al., 2019), while at low concentrations, mt-H_2S has cytoprotective effects, increasing mitochondrial biogenesis and function (Fox et al., 2021). As in the above-mentioned systems, mt-H_2S can act as an inorganic electron donor and interact with mETC components (Módis et al., 2016; Vitvitsky et al., 2018), we analysed the possibility of a link between stomatal closure induction and mETC activity. It has been reported that the activity of the mitochondrial complex II (succinate dehydrogenase [SDH]) is related to stomatal behaviour. The heterozygous mutant *SDH1-1/sdh1-1* and a line with down-regulation of *SHD1-1* expression by RNA interference showed an increased stomatal conductance and stomatal aperture (Fuentes et al., 2011).

In our experimental system, either the inhibition of mitochondrial ETC complex IV or the mutation of both *CYTC-1* and *CYTC-2* genes, impaired AP39-dependent stomatal closure, suggesting that mt-H_2S affects the last steps of mitochondrial ETC. Given that CYTc not only carries electrons to complex IV, but it is also required for the stability of this supercomplex (Welchen et al., 2012), further evidence will be needed to determine whether CYTc, complex IV, or both of them, are involved in the mt-H_2S-triggered signaling pathway. These results can be associated with experiments done in human

cells, where H_2S stimulates O_2 consumption even in the presence of AA, consistently with the entry of electrons at the level of complex IV (Vitvitsky et al., 2018).

Mitochondrial ATP production by oxidative phosphorylation (OXPHOS) has a major relevance in most eukaryotic cells as the main energetic source to drive cellular processes. OXPHOS implies the electron transport from reducing equivalents to molecular oxygen, through the mETC, establishing the Δψm required for ATP synthesis (Braun, 2020). Using the fluorescent probe TMRM in Arabidopsis mito-GFP epidermal peels, we show that AP39 hyperpolarizes Δψm in GCs (Fig. 4). The increase in mitochondrial inner membrane potential, together with the requirement of CYTc/complex IV for AP39-dependent stomatal closure, suggests that mt-H_2S modulates mETC activity, pointing to a relation between mitochondrial function and stomatal movement regulation.

Cytosolic ATP pool in GCs plays a key role for light-dependent stomatal opening (Inoue and Kinoshita, 2017). ATP is needed to fuel plasma membrane H^+-ATPase, which generates the electrochemical gradient that activates inward rectifying K^+ channels, increasing GC's turgor and finally opening the stomatal pore. Recent works suggested that mitochondria are the main ATP source in GCs (Lim et al., 2022), and that plasma membrane H^+-ATPase AHA2 is required for ABA-induced stomatal closure (Pei et al., 2022), highlighting the relevance of mitochondrial energetic metabolism for stomatal physiology.

On the other hand, although ATP requirement for stomatal closure is less explored, the inhibition of mitochondrial ATP synthase, partially inhibits dark-mediated stomatal closure (Goh et al., 2011), indicating that mitochondrial ATP production participates in this response. Our data shows that GC cytosolic ATP levels increase in response to the mt-H_2S donor (Fig. 5). The shift on the Venus/CFP ratio was consistent and reproducible and is in the range of the reported biosensor response to adenine in Arabidopsis seedlings (de Col et al., 2017). Therefore, we provide insights on the relation between mitochondrial ATP production and stomatal closure induction.

Recent reports indicate that H_2S triggers stomatal closure through persulfidation of highly connected components (nodes) that includes the NADPH oxidase Respiratory Burst Oxidase Homolog D (RBOHD) (Shen et al., 2020). Persulfidation promotes RBOHD activity, stimulating the apoplastic superoxide production. Superoxide is rapidly converted to H_2O_2 either spontaneously or by the activity of superoxide dismutase (Chen and Yang, 2020), and then H_2O_2 is believed to enter guard cells trough aquaporins (Rodrigues et al., 2017). In addition, the treatment of epidermal peels with general H_2S donors (NaHS and GYY4137) produces an increase in cytosolic H_2O_2 levels in GCs (Scuffi et al., 2018), showing an interplay between ROS and H_2S. On the other hand, in the last years some works have shown that mitochondrial activity is related to RBOHs-dependent ROS production. The mitochondrial enzyme NAD kinase-CaM dependent (NADKc) catalyzes $NADP^+$ production exclusively in the presence of CaM/Ca^{2+}. The insertional mutants in NADKc, *nadkc-1* and *nadkc-2*, displayed a substantial reduction of extracellular ROS accumulation when seedlings were treated with the pathogen-derived peptide flagellin (flg22) (Dell'Aglio et al., 2019). Authors proposed that the NADKc-dependent NADP(H) synthesis is needed to sustain ROS burst driven by plasma membrane NADPH oxidases. Furthermore, Fabro and colleagues reported the same altered response in ROS production in plants mutated in the enzyme PROLINE DEHYDROGENASE (ProDH), which transfer electrons into the mETC (Fabro et al., 2016). Despite ROS accumulation is a key mechanism that has been observed downstream of several signals that trigger stomatal closure (Arnaud and Hwang, 2015; Zhang et al., 2017; Postiglione and Muday, 2020), there are no reports showing the participation of mitochondrial activity on ROS production in GCs. Based on these pieces of evidence that connect mitochondrial function with ROS accumulation, together with the, well stablished, interplay between H_2S and H_2O_2 in GCs, we analysed cytosolic H_2O_2 content and the GSH/GSSH ratio. In Figure 6 we show that AP39 triggers the oxidation of both roGFP2-Orp1 and Grx1-roGFP2 sensors, but their dynamics are different. After reaching a maximum oxidation at 10 min, Grx1-roGFP2 was fully reduced back to its initial state. These results indicate that the mt-H_2S donor increases the H_2O_2 levels and the oxidation

of the GSH pool in GCs, pointing to a signaling role of mitochondrial H_2S over cytosolic components in the regulation of stomatal closure. Although it is tempting to link the raise of cytosolic H_2O_2 to its reported effect on inward-rectifying K^+ channels (I_{KIN}) activity (Köhler et al., 2003), it is difficult to propose a linear pathway in such a complex signaling network.

Based in our findings, we propose that mitochondrially-targeted H_2S delivery molecule AP39 induces stomatal closure, a response that depends on a functional CYTc or/and complex IV. Additionally, this donor also hyperpolarizes the mitochondrial inner membrane, increases the cytosolic GSH oxidation, and the ATP and H_2O_2 content in GCs (Fig. 7). Taken together, these results point towards an effect of mt-H_2S over mETC at the CYTc/complex IV level that induces an increase in the mitochondrial inner membrane potential and an increase in the ATP synthesis in GCs. The modulation of mitochondrial activity by AP39 can possibly lead to the spread of the signal to other cellular compartments, increasing the oxidation of GSH pool and the H_2O_2 levels in GCs, finally producing stomatal closure. These observations indicate that mt-H_2S has a function in the modulation of mitochondrial energetics in plants, while they also point to an active role of mitochondrial activity in stomatal closure. Nevertheless, more studies are required to unveil the gap between the mitochondrial effect of AP39 and the cytosolic H_2O_2 increase in GCs, as well as the relevance of this signaling pathway in a physiological context to further understand the mitochondrial role in GC's signaling network.

MATERIALS AND METHODS

Plant material and Chemicals

Arabidopsis (*Arabidopsis thaliana*) wild-type Columbia-0 (Col-0) ecotype, Arabidopsis mito-GFP, Arabidopsis CYTc mutants *1*a, *1*b, *2*a, *2*b, *1*b*2*a and *1*b*2*b (Welchen et al., 2012) , and Arabidopsis lines expressing the biosensors ATeam1.03-nD/nA (de Col et al., 2017), roGFP2-Orp1 and Grx1-roGFP2 (Gutscher et al., 2009; Nietzel et al., 2019) (kindly provided by Prof. Markus

Schwarzländer) were grown in soil:perlite:vermiculite (1:1:1, v/v/v); while fava bean (*Vicia faba* were grown in soil:vermiculite (1:3 v/v). All plants were placed at 20°C under short-day conditions (8-h- light/16-h-dark photoperiod, 200 µmol photons m^{-2} s^{-1}), after stratification for 48 hours at 4°C in the dark.

Mitochondrial H_2S donors AP123 (Gerő et al., 2016b) (10-(4-carbamothioylphenoxy)-10-oxodecyl) triphenylphosphonium bromide), AP39 (le Trionnaire et al., 2014), ((10-oxo-10-(4-(3-thioxo-3H-1,2-dithiol-5-yl)phenoxy) decyl) triphenylphosphonium bromide) and RT01 (Latorre et al., 2018) were synthesized as previously described by us. GYY4137 (morpholin-4-ium4 methoxyphenyl(morpholino) phosphinodithioate) was purchased from Sigma-Aldrich. Rotenone, 2-Thenoyltrifluoroacetone (TTFA) and Antimycin A (AA) were purchased from Tecnolab S.A., while Potassium cyanide (KCN) was purchased from Mallinckrodt Pharmaceuticals. Tetramethylrhodamine methyl ester (TMRM) was purchased from Biotium.

Stomatal Aperture measurements

Epidermal peels were excised from abaxial side of 5-6 weeks old *Arabidopsis thaliana* Col-0 or 4-weeks old *Vicia faba* leaves and immediately floated in Opening Buffer (OB: 5 mM MES-KOH, 50 mM KCl, pH=6.1) for 3 hours in the light. Strips were then kept in the same OB and exposed to different treatments as indicated in the figure legends. Stomata were digitized using an AmScope MU1000 camera coupled to an Olympus CKX53 microscope with a 40x lens (LUCPlanFLN, 0.6 numerical aperture). The stomatal aperture was measured using IMAGEJ analysis software (NIH, Bethesda, MD, USA).

Viability staining

Arabidopsis Col-0 epidermal strips were incubated for 3 hours in OB in light and exposed to different treatments. Then, peels were incubated with 20 µM fluorescein diacetate (FDA) for 10 minutes in the dark at room temperature and washed with fresh OB to remove excess dye. Fluorescence was imaged with a 40x lens (LUCPlanFLN, 0.6 numerical aperture) using an Amscope MU900 camera coupled to an Olympus CKX41 microscope equipped with an Olympus U-RFLT50 lamp, a BP460-490C excitation filter and a BA520 IF barrier filter. Exposure times (from 100ms to 300 ms) were adjusted depending on the probe fluorescence intensity in each experiment.

Confocal microscopy

Fluorescence images were acquired with a Nikon Eclipse C1 Plus confocal microscope. Mitochondria in guard cells were imaged with a 100x lens (Plan Apochromat Lambda, 1.45 numerical aperture, oil immersion). Epidermal peels from *Arabidopsis thaliana* expressing a mitochondrial-targeted GFP (mito-GFP) were floated in OB supplemented with 500 nM Tetramethylrhodamine methyl ester (TMRM) for 3 hours in the dark and then treated for 90 minutes with Mock (DMSO 0.01% (v/v)) or 100 nM AP39. TMRM and GFP were excited at 488 nm and 561 nm respectively, and their emissions were collected simultaneously at 515/30 and 605/75nm. The laser intensity was set to 4% for 488nm and 5% for 561nm. The ratio TMRM/GFP was calculated for each GC and the values were normalized to the Mock.

Fluorescence Microscopy

Guard cells of plants expressing ATeam1.03-nD/Na, roGFP2-Orp1 and Grx1-roGFP2 biosensors were analyzed *in vivo* using an inverted Nikon Ti-E fluorescence microscope coupled to a Hamamatsu ORCA-D2 Dual CCD camera. Excitation light was produced by a fluorescent lamp Prior Lumen 200 PRO (Prior Scientific) and epidermal strips were imaged using a 60x oil immersion objective (CFI Plan APO Lambda 60x 1.4 numerical aperture). Epidermal peels from ATeam1.03-nD/nA leaves were floated in OB a least 1 hour in the dark and then treated for 1 hour with DMSO 0.01% (v/v) (Mock) or 100 nM AP39. Peels were excited at 440 nm (436/20 nm), and mseCFP and cp173-mVenus emissions were collected at 483/32 nm and 542/27 nm, respectively, with a dichroic 510-nm mirror (Hamamatsu Pho-tonics) for simultaneous acquisitions. Exposure times (from 150ms to 200 ms) were adjusted depending on the sensor expression level in each experiment, with a 4 x 4 pixel binning. The ratio Venus/CFP was calculated for each GC and the values were normalized to the Mock.

roGFP2-Orp1 and Grx1-roGFP2 peels were floated in OB at least 7 hours in light and then treated with DMSO 0.01% (v/v) (Mock), 100 nM AP39, or AP39 and 200 µM HT for the indicated times. Sensors were excited sequentially with 470/40 nm and 405/40 nm and the emissions were collected using a 505/530 nm bandpass filter (GFP-specific filter) for both excitation wavelengths with a 2 x 2 pixel binning. For roGFP2-Orp1 and Grx1-roGFP2 experiments, the exposure times were 100ms and 200ms, and 50ms and 200ms, for 405/40 nm and 470/40 nm excitations,

respectively. The ratio 405/488nm was calculated for each GC and the values were normalized to the Mock.

Images analysis

Images were analysed using IMAGEJ software (NIH, Bethesda, MD, USA). For TMRM/GFP ratio calculation and fluorescence measurement from roGFP2-Orp1, Grx1-roGFP2 and ATeam1.03-nD/nA sensors, the background was subtracted from each channel and then the region of interest was delimited to GCs. Fluorescence was measured as the mean pixel intensity.

To obtain the ratiometric false-colored ATeam1.03-nD/nA images, background was subtracted to mseCFP and cp173-mVenus emissions in representative images, and then they were thresholded. Finally, cp173-mVenus/mseCFP (Venus/CFP in Figure 5) was generated with Image Calculator and a pseudocolor (LUT Physics) was applied to the resulting image.

Statistical Analyses

Data analyses were performed using RStudio (R Foundation for Statistical Computing, Vienna, Austria. URL: https://www.R-project.org/). The statistically significant differences were analyzed using Student's t test, Tukey's Method or Dunnett's Method, as indicated in the figure legends.

Accession Numbers

Sequence data from this article can be found in the GenBank/EMBL data libraries under accession numbers At1g22840 (*CYTC-1*) and At4g10040 (*CYTC-2*).

Funding information

This work was financially supported by Universidad Nacional de Mar del Plata (UNMDP), Consejo Nacional de Investigaciones Científicas y Técnicas (CONICET), Agencia Nacional de Promoción Científica y Tecnológica and The Company of Biologists. PICT 2016 N°2553 (to CGM) PICT 2018 N°1986 (to CGM) and PICT 2018 N°1449 (to DS), PhD finishing fellowship from CONICET (to RP), and Travelling Fellowship from The Company of Biologists (to RP).

Acknowledgments

We thank to Ana M. Laxalt and the members of the Signaling Mechanisms in Plants Lab for the challenging discussion.

Conflicts of Interest

M.W and R.T. have intellectual property (patents awarded) on mitochondrial and other targeted H_2S donors and MW is CSO of MitoRx Therapeutics.

Figure legends

Figure 1. The mitochondrial H_2S donor AP39 induces stomatal closure in a dose-dependent manner. Epidermal strips were excised from abaxial side from 5-6 weeks old Arabidopsis (*Arabidopsis thaliana*) leaves (ecotype Columbia -Col-0) and floated in opening buffer (OB: 5 mM MES, 50 mM KCl, pH=6.1) for 3 hours in the light. Then, they were treated for 90 minutes with Dimethyl sulfoxide (DMSO) 0.01% (v/v) (Mock), 100 µM of general H_2S donor GYY4137, 100 nM AP39 and 200 µM of the H2S scavenger hypotaurine (HT), or with increasing concentrations of mitochondrial H_2S donor AP39. Stomatal aperture was measured (A,C), or AP39-treated peels were subsequently loaded with the fluorescent dye Fluorescein diacetate (FDA) (B). Stomatal aperture values are expressed as absolute values in microns (µm) and are represented as points in the boxplots, where the box is bound by the 25th to 75th percentile (A). The line in the middle is the median, the darker point is the mean and whiskers span 10th to 90th percentile. The black points are outliers. The percentage of guard cell viability is the result of the ratio between fluorescent guard cells and total guard cells in the bright field (B). The bars represent the means, and the points are individual measurements. Error bars = SD. Data is from at least three independent assays. Letters indicate statistical differences among treatments (Tukey's Method, confidence level=0.95) (A,C). Asterisks indicate statistical differences from the Mock (Dunnett's Method, p-value<0.05 = (*), confidence level=0.95) (B).

Figure 2. AP39-induced stomatal closure requires complex IV activity. (A) Scheme showing the sites of action of the different mitochondrial electron transport chain (mETC) inhibitors; Epidermal strips from the abaxial side of 5-6 weeks old Arabidopsis Col-0 leaves were floated in OB (5 mM MES, 50 mM KCl, pH=6.1) for 3 hours in the light and then they were treated with Dimethyl sulfoxide (DMSO) 0.01% (v/v) (Mock), 100 nM AP39, or they were pre-incubated for 30

minutes with the different mETC inhibitors: (B) 1 µM Rotenone (Rtn), (C) 100 µM 2-Thenoyltrifluoroacetone (TTFA), (D) 50 µM Antimycin A (AA) or (E) 1 mM potassium cyanide (KCN), and subsequently treated or not with AP39 for 90 minutes. The values of stomatal aperture are expressed in microns (µm) and are represented as points in the boxplots where the box is bound by the 25th to 75th percentile. The line in the middle is the median, the darker point is the mean and whiskers span 10th to 90th percentile. The black points represent outliers. Data is the result from at least three independent assays. Letters indicate statistical differences among treatments (Tukey's Method, confidence level=0.95). IMS: intermembrane space.

Figure 3. AP39-induced stomatal closure involves cytochrome c (CYTc). Epidermal strips from the abaxial side of leaves of 5-6 weeks old Arabidopsis double or single insertional mutants in cytochrome *c CYTC-1* and *CYTC-2* (*1*b*2*a and *1*b*2*b (A), *1*a and *1*b (B), or *2*a and *2*b (C)), were floated in OB (5 mM MES, 50 mM KCl, pH=6.1) for 3 hours in the light. Then, they were treated for 90 minutes with Dimethyl sulfoxide (DMSO) 0.01% (v/v) (Mock) or 100 nM AP39. The values of stomatal aperture width are expressed in microns (µm) and are represented as points in the boxplots where the box is bound by the 25th to 75th percentile. The line in the middle is the median, the darker point is the mean and whiskers span 10th to 90th percentile. The black points are outliers. Data is from at least three independent assays. Asterisks indicate statistical differences with the Mock (Student's t-test, confidence level=0.95 (p-value<0.05 = (*), p-value<0.01 = (**), p-value<0.001 = (***), NS=Not significant).

Figure 4. AP39 hyperpolarizes mitochondrial inner membrane potential in guard cells. Epidermal peels from abaxial side of 5-6 weeks old Arabidopsis mito-GFP leaves were incubated in OB (5 mM MES, 50 mM KCl, pH=6.1) with 500 nM Tetramethylrhodamine methyl ester (TMRM) in the dark, and then treated with Dimethyl sulfoxide (DMSO) 0.01% (v/v) (Mock) or 100 nM AP39 for 90 minutes. (A) Representative false-colored images of guard cells treated with the Mock or AP39. (B) The ratios between TMRM and GFP fluorescence intensities (TMRM/GFP) were calculated for each guard cell, normalised to the Mock and represented as individual points in the boxplots, where the box is bound by the 25th to 75th percentile. The line in the middle is the median, the darker point is the mean and whiskers span 10th to 90th percentile. The black points are outliers. Data is for at least 30 guard cells per treatment and three independent assays.

Asterisks indicate statistical differences with the Mock (Student's t-test, confidence level=0.95 (p-value<0.05 = (*)). Scale bars: 5 µm.

Figure 5. AP39 increases cytosolic $MgATP^{-2}$ levels in guard cells. Epidermal strips from abaxial side of 5-6 weeks old Arabidopsis Col-0 leaves expressing the cytosolic $MgATP^{-2}$ sensor ATeam1.03-nD/Na were placed in OB (5 mM MES, 50 mM KCl, pH=6.1), dark-adapted at least 60 minutes and treated for 90 minutes with Dimethyl sulfoxide (DMSO) 0.01% (v/v) (Mock) or 100 nM AP39. (A) Representative false-colored ratiometric images of guard cells treated with the Mock or AP39. (B) The ratio between Venus and CFP fluorescence intensities (Venus/CFP) were calculated for each guard cell, normalised to the Mock and represented as individual points in the boxplots, where the box is bound by the 25^{th} to 75^{th} percentile. The line in the middle is the median, the darker point is the mean and whiskers span 10^{th} to 90^{th} percentile. The black points are outliers. Data is the result of at least 70 guard cells for each treatment from three independent assays. Asterisks indicate statistical differences with the Mock (Student's t-test, confidence level=0.95 (p-value<0.01 = (**)). Scale bars: 5 µm.

Figure 6. AP39 oxidizes cytosolic roGFP2-Orp1 and Grx1-roGFP2 in guard cells. Epidermal peels from Arabidopsis Col-0 leaves expressing the cytosolic biosensors that detect H_2O_2 and the glutathione (GSH) oxidative state, roGFP2-Orp1 (A,C) or Grx1-roGFP2 (B), respectively, were incubated in opening buffer (OB: 5 mM MES, 50 mM KCl, pH=6.1) for 7 h under light and then treated with: Dimethyl sulfoxide (DMSO) 0.01% (v/v) (Mock) for 60 minutes, 100 nM AP39 for 5, 10, 15, 20, 30 or 60 minutes, 20 mM Dithiothreitol (DTT) for 10 minutes, 1 mM H_2O_2 for 10 minutes, or 200 µM Hypotaurine (HT) and AP39 for 60 minutes. The ratios between emissions collected with 405/488 nm excitations were calculated for each guard cell, normalised to the Mock and represented as individual points in the boxplots, where the box is bound by the 25^{th} to 75^{th} percentile. The line in the middle is the median, the darker point is the mean and whiskers span 10^{th} to 90^{th} percentile. The black points are outliers. Data is the result of at least three independent assays. Asterisks indicate statistical differences with the Mock (Dunnett's test = (p-value<0.05 = (*), p-value<0.01 = (**), p-value<0.001 = (***)). Ratiometric images are false-colored and represent the different treatments. Scale bars: 5 µm.

Figure 7. Model of mitochondrial (mt)-H_2S-triggered signaling pathway in guard cells. The donor AP39 accumulates in mitochondria and releases mitochondrial (mt)-H_2S, triggering a signaling pathway that concludes in stomatal closure. To induce the reduction of stomatal pore size, AP39 requires the activity of cytochrome *c* (CYTc) and/or mitochondrial complex IV. Further, AP39 hyperpolarizes the mitochondrial membrane potential (Δψm) and increases ATP synthesis in guard cells, as well as the cytosolic H_2O_2 levels and the oxidation of the glutathione (GSH) pool. Segmented lines suggest a possible participation of H_2O_2, GSH, ATP and Δψm on stomatal closure induction, which can be modulated through CYTc/complex IV.

References

Araújo, W. L., Nunes-Nesi, A., Osorio, S., Usadel, B., Fuentes, D., Nagy, R., Balbo, I., Lehmann, M., Studart-Witkowski, C., Tohge, T., Martinoia, E., Jordana, X., DaMatta, F. M., & Fernie, A. R. (2011). Antisense inhibition of the iron-sulphur subunit of succinate dehydrogenase enhances photosynthesis and growth in tomato via an organic acid-mediated effect on stomatal aperture. Plant Cell, 23(2), 600–627. https://doi.org/10.1105/tpc.110.081224

Arnaud D, Hwang I (2015) A Sophisticated Network of Signaling Pathways Regulates Stomatal Defenses to Bacterial Pathogens. Mol Plant **8**: 566–581

Aroca A, Gotor C, Bassham DC, Romero LC (2020) Hydrogen sulfide: From a toxic molecule to a key molecule of cell life. Antioxidants **9**: 1–24

Baudouin E, Poilevey A, Hewage NI, Cochet F, Puyaubert J, Bailly C (2016) The significance of hydrogen sulfide for arabidopsis seed germination. Front Plant Sci. doi: 10.3389/fpls.2016.00930

Benchoam D, Cuevasanta E, Möller M, Alvarez B (2019) Hydrogen Sulfide and Persulfides Oxidation by Biologically Relevant Oxidizing Species. Antioxidants **8**: 48

Brand MD, Nicholls DG (2011) Assessing mitochondrial dysfunction in cells. Biochemical Journal **435**: 297–312

Braun H-P (2020) The Oxidative Phosphorylation system of the mitochondria in plants. Mitochondrion **53**: 66–75

Chen Q, Yang G (2020) Signal Function Studies of ROS, Especially RBOH-Dependent ROS, in Plant Growth, Development and Environmental Stress. J Plant Growth Regul **39**: 157–171

de Col, V., Fuchs, P., Nietzel, T., Elsässer, M., Voon, C. P., Candeo, A., Seeliger, I., Fricker, M. D., Grefen, C., Møller, I. M., Bassi, A., Lim, B. L., Zancani, M., Meyer, A. J., Costa, A., Wagner, S., & Schwarzländer, M. (2017). ATP sensing in living plant cells reveals tissue gradients and stress dynamics of energy physiology. ELife, 6. https://doi.org/10.7554/eLife.26770

Covarrubias AE, Lecarpentier E, Lo A, Salahuddin S, Gray KJ, Karumanchi SA, Zsengellér ZK (2019) AP39, a Modulator of Mitochondrial Bioenergetics, Reduces Antiangiogenic Response and Oxidative Stress in Hypoxia-Exposed Trophoblasts: Relevance for Preeclampsia Pathogenesis. American Journal of Pathology 189: 104–114

Daloso DM, Antunes WC, Pinheiro DP, Waquim JP, Araújo WL, Loureiro ME, Fernie AR, Williams TCR (2015) Tobacco guard cells fix CO2 by both Rubisco and PEPcase while sucrose acts as a substrate during light-induced stomatal opening. Plant Cell Environ **38**: 2353–2371

Dell'Aglio, E., Giustini, C., Kraut, A., Couté, Y., Costa, A., Decros, G., Gibon, Y., Mazars, C., Matringe, M., Finazzi, G., & Curien, G. (2019). Identification of the Arabidopsis Calmodulin-

Dependent NAD + Kinase That Sustains the Elicitor-Induced Oxidative Burst. Plant Physiology, 181(4), 1449–1458. https://doi.org/10.1104/pp.19.00912

Fabro G, Rizzi YS, Alvarez ME (2016) *Arabidopsis* Proline Dehydrogenase Contributes to Flagellin-Mediated PAMP-Triggered Immunity by Affecting RBOHD. Molecular Plant-Microbe Interactions® **29**: 620–628

Filipovic MR, Zivanovic J, Alvarez B, Banerjee R (2018) Chemical Biology of H2S Signaling through Persulfidation. Chem Rev **118**: 1253–1337

Fox BC, Slade L, Torregrossa R, Pacitti D, Szabo C, Etheridge T, Whiteman M (2021a) The mitochondria-targeted hydrogen sulfide donor AP39 improves health and mitochondrial function in a <scp> *C. elegans* </scp> primary mitochondrial disease model. J Inherit Metab Dis **44**: 367–375

Fu M, Zhang W, Wu L, Yang G, Li H, Wang R (2012) Hydrogen sulfide (H_2S) metabolism in mitochondria and its regulatory role in energy production. Proceedings of the National Academy of Sciences **109**: 2943–2948

García I, Castellano JM, Vioque B, Solano R, Gotor C, Romero LC (2010) Mitochondrial β-Cyanoalanine Synthase Is Essential for Root Hair Formation in *Arabidopsis thaliana* . Plant Cell **22**: 3268–3279

García-Mata C, Lamattina L (2013) Gasotransmitters are emerging as new guard cell signaling molecules and regulators of leaf gas exchange. Plant Science **201–202**: 66–73

García-Mata C, Lamattina L (2010) Hydrogen sulphide, a novel gasotransmitter involved in guard cell signalling. New Phytologist **188**: 977–984

Gerő D, Torregrossa R, Perry A, Waters A, Le-Trionnaire S, Whatmore JL, Wood M, Whiteman M (2016a) The novel mitochondria-targeted hydrogen sulfide (H2S) donors AP123 and AP39 protect against hyperglycemic injury in microvascular endothelial cells in vitro. Pharmacol Res **113**: 186–198

Goh CH, Ko SM, Park Y il, Kim CS, Song KJ (2011) Regulation of Dark-Induced Stomatal Closure in Arabidopsis Dynamin-Like Protein 1E (adl1e) Mutant Leaves. Journal of Plant Biology **54**: 112–118

Gutscher M, Sobotta MC, Wabnitz GH, Ballikaya S, Meyer AJ, Samstag Y, Dick TP (2009) Proximity-based Protein Thiol Oxidation by H2O2-scavenging Peroxidases. Journal of Biological Chemistry **284**: 31532–31540

Hetherington AM, Woodward FI (2003) The role of stomata in sensing and driving environmental change. Nature **424**: 901–908

Horrer D, Flütsch S, Pazmino D, Matthews JSA, Thalmann M, Nigro A, Leonhardt N, Lawson T, Santelia D (2016) Blue light induces a distinct starch degradation pathway in guard cells for stomatal opening. Current Biology **26**: 362–370

Imamura, H., Huynh Nhat, K. P., Togawa, H., Saito, K., Iino, R., Kato-Yamada, Y., Nagai, T., & Noji, H. (2009). Visualization of ATP levels inside single living cells with fluorescence resonance energy transfer-based genetically encoded indicators. *Proceedings of the National Academy of Sciences*, *106*(37), 15651–15656. https://doi.org/10.1073/pnas.0904764106

Inoue S, Kinoshita T (2017) Blue Light Regulation of Stomatal Opening and the Plasma Membrane H^+-ATPase. Plant Physiol **174**: 531–538

Köhler, B., Hills, A., & Blatt, M. R. (2003). Control of Guard Cell Ion Channels by Hydrogen Peroxide and Abscisic Acid Indicates Their Action through Alternate Signaling Pathways. Plant Physiology, 131(2), 385–388. https://doi.org/10.1104/pp.016014

Kotera, I., Iwasaki, T., Imamura, H., Noji, H., & Nagai, T. (2010). Reversible Dimerization of *Aequorea victoria* Fluorescent Proteins Increases the Dynamic Range of FRET-Based Indicators. *ACS Chemical Biology*, *5*(2), 215–222. https://doi.org/10.1021/cb900263z

Latorre E, Torregrossa R, Wood ME, Whiteman M, Harries LW (2018) Mitochondria-targeted hydrogen sulfide attenuates endothelial senescence by selective induction of splicing factors HNRNPD and SRSF2. Aging **10**: 1666–1681

Laureano-Marín AM, Aroca Á, Pérez-Pérez ME, Yruela I, Jurado-Flores A, Moreno I, Crespo JL, Romero LC, Gotor C (2020) Abscisic acid-triggered persulfidation of the cys protease ATG4 mediates regulation of autophagy by sulfide. Plant Cell **32**: 3902–3920

Lawson T, Matthews J (2020) Guard Cell Metabolism and Stomatal Function. doi: 10.1146/annurev-arplant-050718

Lim SL, Flütsch S, Liu J, Distefano L, Santelia D, Lim BL (2022) Arabidopsis guard cell chloroplasts import cytosolic ATP for starch turnover and stomatal opening. Nat Commun. doi: 10.1038/s41467-022-28263-2

Lisjak M, Srivastava N, Teklic T, Civale L, Lewandowski K, Wilson I, Wood ME, Whiteman M, Hancock JT (2010) A novel hydrogen sulfide donor causes stomatal opening and reduces nitric oxide accumulation. Plant Physiology and Biochemistry **48**: 931–935

Logan DC, Leaver CJ (2000) Mitochondria-targeted GFP highlights the heterogeneity of mitochondrial shape, size and movement within living plant cells. J Exp Bot **51**: 865–871

McLachlan, D. H., Lan, J., Geilfus, C. M., Dodd, A. N., Larson, T., Baker, A., Hõrak, H., Kollist, H., He, Z., Graham, I., Mickelbart, M. v., & Hetherington, A. M. (2016). The Breakdown of Stored Triacylglycerols is Required during Light-Induced Stomatal Opening. Current Biology, 26(5), 707–712. https://doi.org/10.1016/j.cub.2016.01.019

Módis K, Ju YJ, Ahmad A, Untereiner AA, Altaany Z, Wu L, Szabo C, Wang R (2016) S-Sulfhydration of ATP synthase by hydrogen sulfide stimulates mitochondrial bioenergetics. Pharmacol Res **113**: 116–124

Nietzel, T., Elsässer, M., Ruberti, C., Steinbeck, J., Ugalde, J. M., Fuchs, P., Wagner, S., Ostermann, L., Moseler, A., Lemke, P., Fricker, M. D., Müller-Schüssele, S. J., Moerschbacher, B. M., Costa, A., Meyer, A. J., & Schwarzländer, M. (2019). The fluorescent protein sensor ro <scp>GFP</scp> 2-Orp1 monitors in vivo H 2 O 2 and thiol redox integration and elucidates intracellular H 2 O 2 dynamics during elicitor-induced oxidative burst in Arabidopsis. New Phytologist, 221(3), 1649–1664. https://doi.org/10.1111/nph.15550

Olson KR, Straub KD (2016) The Role of Hydrogen Sulfide in Evolution and the Evolution of Hydrogen Sulfide in Metabolism and Signaling. Physiology **31**: 60–72

Panagaki T, Randi EB, Augsburger F, Szabo C (2019) Overproduction of H_2S, generated by CBS, inhibits mitochondrial Complex IV and suppresses oxidative phosphorylation in Down syndrome. Proceedings of the National Academy of Sciences **116**: 18769–18771

Pei, D., Hua, D., Deng, J., Wang, Z., Song, C., Wang, Y., Wang, Y., Qi, J., Kollist, H., Yang, S., Guo, Y., & Gong, Z. (2022). Phosphorylation of the plasma membrane H+-ATPase AHA2 by BAK1 is required for ABA-induced stomatal closure in Arabidopsis. *The Plant Cell*, *34*(7), 2708–2729. https://doi.org/10.1093/plcell/koac106

Postiglione AE, Muday GK (2020) The Role of ROS Homeostasis in ABA-Induced Guard Cell Signaling. Front Plant Sci. doi: 10.3389/fpls.2020.00968

Rodrigues O, Reshetnyak G, Grondin A, Saijo Y, Leonhardt N, Maurel C, Verdoucq L (2017) Aquaporins facilitate hydrogen peroxide entry into guard cells to mediate ABA- and pathogen-triggered stomatal closure. Proceedings of the National Academy of Sciences **114**: 9200–9205

Scuffi D, Álvarez C, Laspina N, Gotor C, Lamattina L, García-Mata C (2014) Hydrogen Sulfide Generated by <scp>l</scp> -Cysteine Desulfhydrase Acts Upstream of Nitric Oxide to Modulate Abscisic Acid-Dependent Stomatal Closure . Plant Physiol **166**: 2065–2076

Scuffi D, Nietzel T, di Fino LM, Meyer AJ, Lamattina L, Schwarzländer M, Laxalt AM, García-Mata C (2018) Hydrogen Sulfide Increases Production of NADPH Oxidase-Dependent Hydrogen Peroxide and Phospholipase D-Derived Phosphatidic Acid in Guard Cell Signaling. Plant Physiol **176**: 2532–2542

Shen, J., Zhang, J., Zhou, M., Zhou, H., Cui, B., Gotor, C., Romero, L. C., Fu, L., Yang, J., Foyer, C. H., Pan, Q., Shen, W., & Xie, Y. (2020). Persulfidation-based Modification of Cysteine Desulfhydrase and the NADPH Oxidase RBOHD Controls Guard Cell Abscisic Acid Signaling. The Plant Cell, 32(4), 1000–1017. https://doi.org/10.1105/tpc.19.00826

Szabo C, Ransy C, Módis K, Andriamihaja M, Murghes B, Coletta C, Olah G, Yanagi K, Bouillaud F (2014) Regulation of mitochondrial bioenergetic function by hydrogen sulfide. Part I. Biochemical and physiological mechanisms. Br J Pharmacol **171**: 2099–2122

le Trionnaire S, Perry A, Szczesny B, Szabo C, Winyard PG, Whatmore JL, Wood ME, Whiteman M (2014) The synthesis and functional evaluation of a mitochondria-targeted hydrogen sulfide donor, (10-oxo-10-(4-(3-thioxo-3H-1,2-dithiol-5-yl)phenoxy)decyl) triphenylphosphonium bromide (AP39). Medchemcomm **5**: 728–736

Vitvitsky, V., Miljkovic, J. Lj., Bostelaar, T., Adhikari, B., Yadav, P. K., Steiger, A. K., Torregrossa, R., Pluth, M. D., Whiteman, M., Banerjee, R., & Filipovic, M. R. (2018). Cytochrome c Reduction by H 2 S Potentiates Sulfide Signaling. ACS Chemical Biology, 13(8), 2300–2307. https://doi.org/10.1021/acschembio.8b00463

Welchen E, Gonzalez DH (2016) Cytochrome c , a hub linking energy, redox, stress and signaling pathways in mitochondria and other cell compartments. Physiol Plant **157**: 310–321

Welchen E, Hildebrandt TM, Lewejohann D, Gonzalez DH, Braun H-P (2012) Lack of cytochrome c in Arabidopsis decreases stability of Complex IV and modifies redox metabolism without affecting Complexes I and III. Biochimica et Biophysica Acta (BBA) - Bioenergetics **1817**: 990–1001

Wille AC, Lucas WJ (1984) Ultrastructural and histochemical studies on guard cells. Planta **160**: 129–142

Willmer C, Fricker M (1996) Stomata. J Chem Inf Model. doi: 10.1007/978-94-011-0579-8

Zhang T-Y, Li F-C, Fan C-M, Li X, Zhang F-F, He J-M (2017) Role and interrelationship of MEK1-MPK6 cascade, hydrogen peroxide and nitric oxide in darkness-induced stomatal closure. Plant Science **262**: 190–199

Zorova LD, Popkov VA, Plotnikov EJ, Silachev DN, Pevzner IB, Jankauskas SS, Zorov SD, Babenko VA, Zorov DB (2018) Functional Significance of the Mitochondrial Membrane Potential. Biochem (Mosc) Suppl Ser A Membr Cell Biol **12**: 20–26

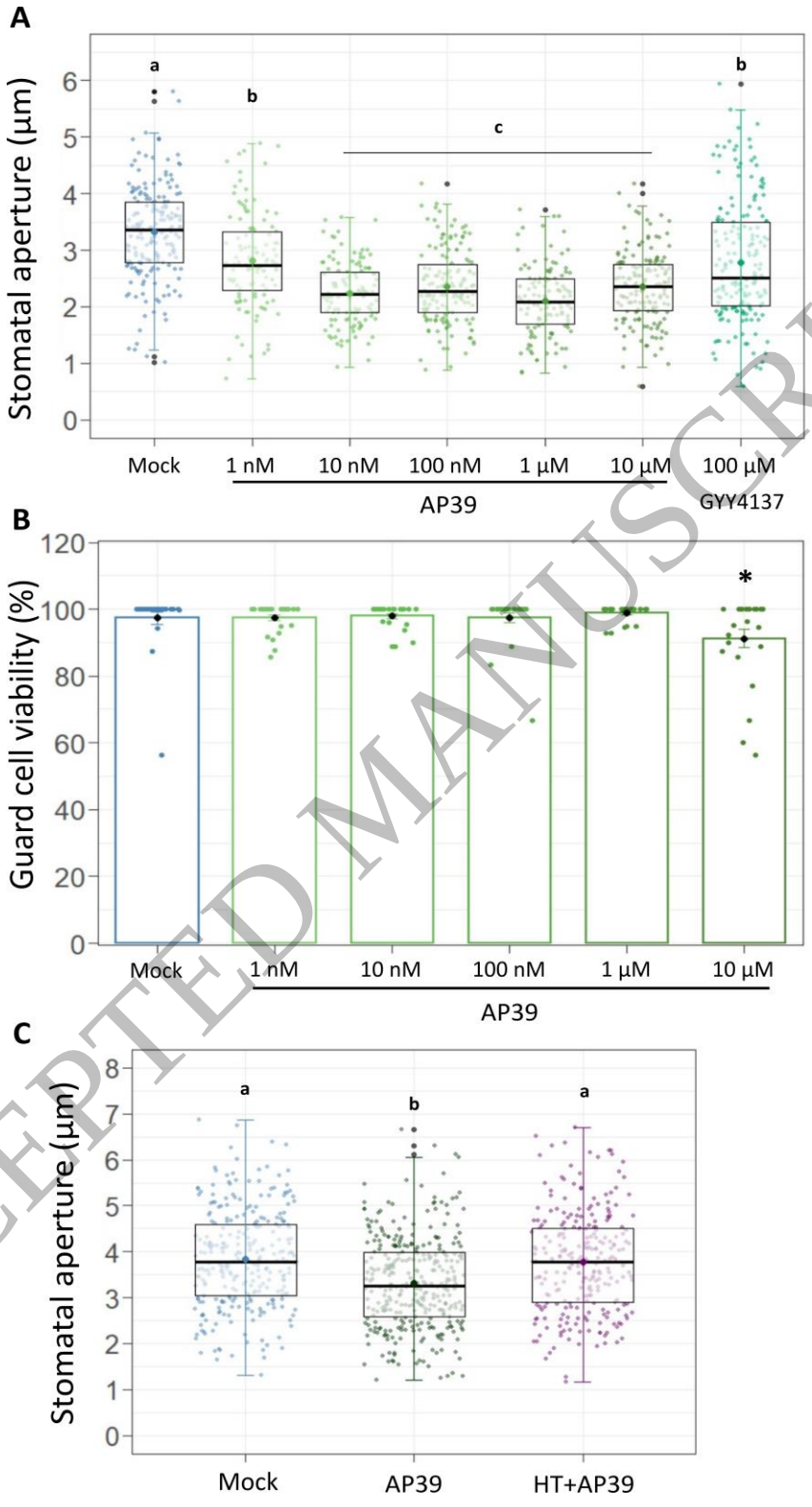

Figure 1
128x247 mm (3.2 x DPI)

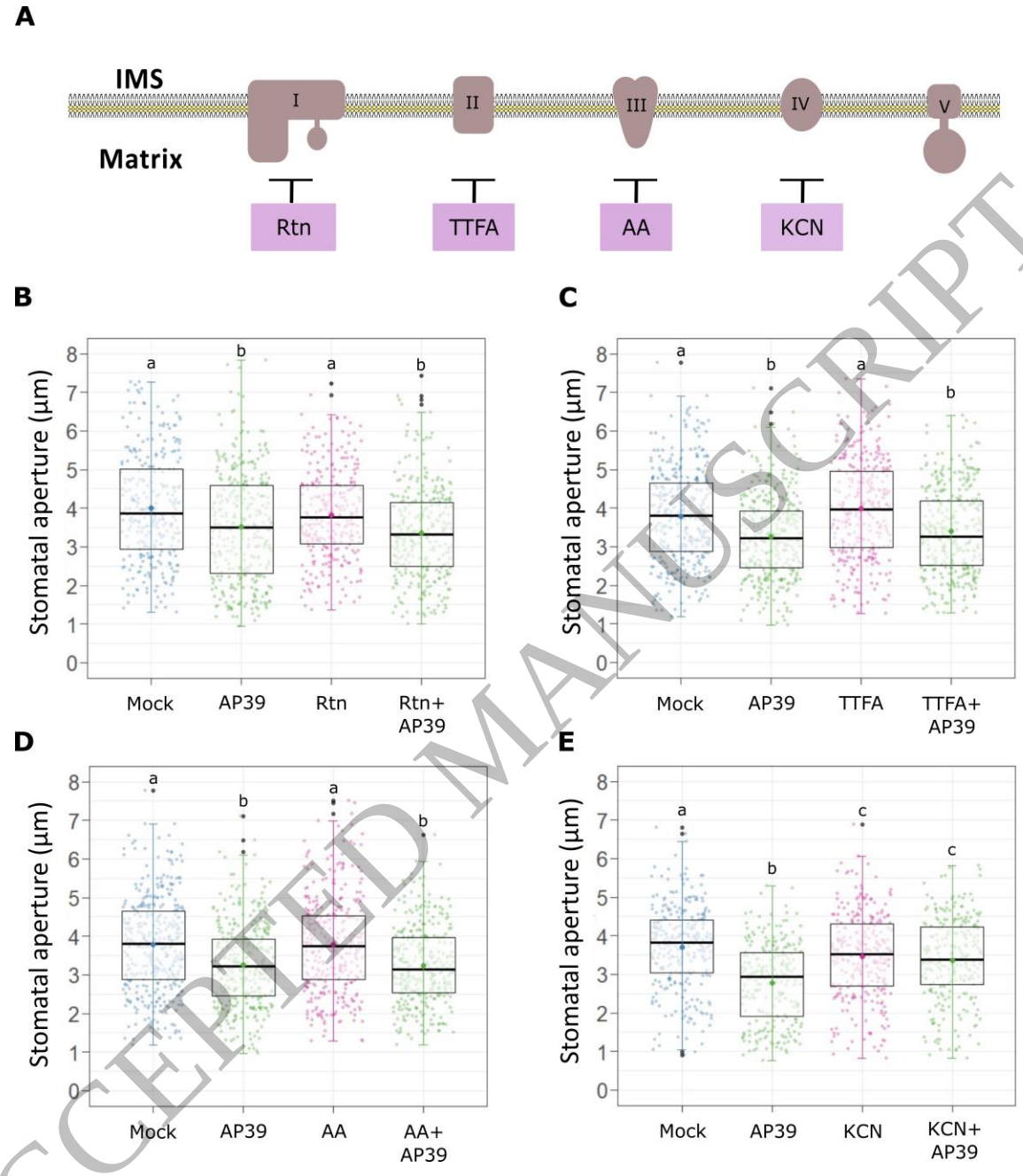

Figure 2
150x172 mm (3.2 x DPI)

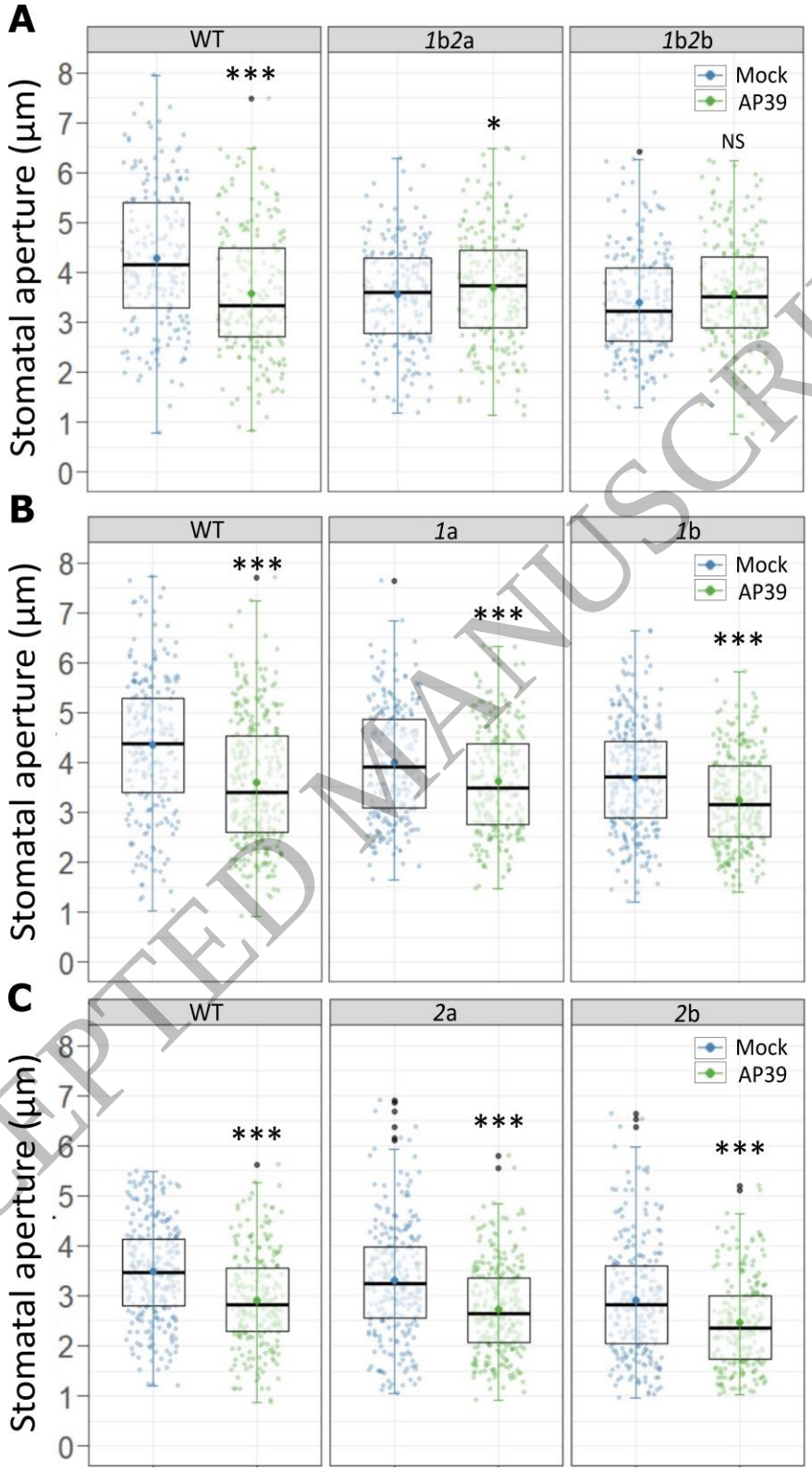

Figure 3
142x247 mm (3.2 x DPI)

1

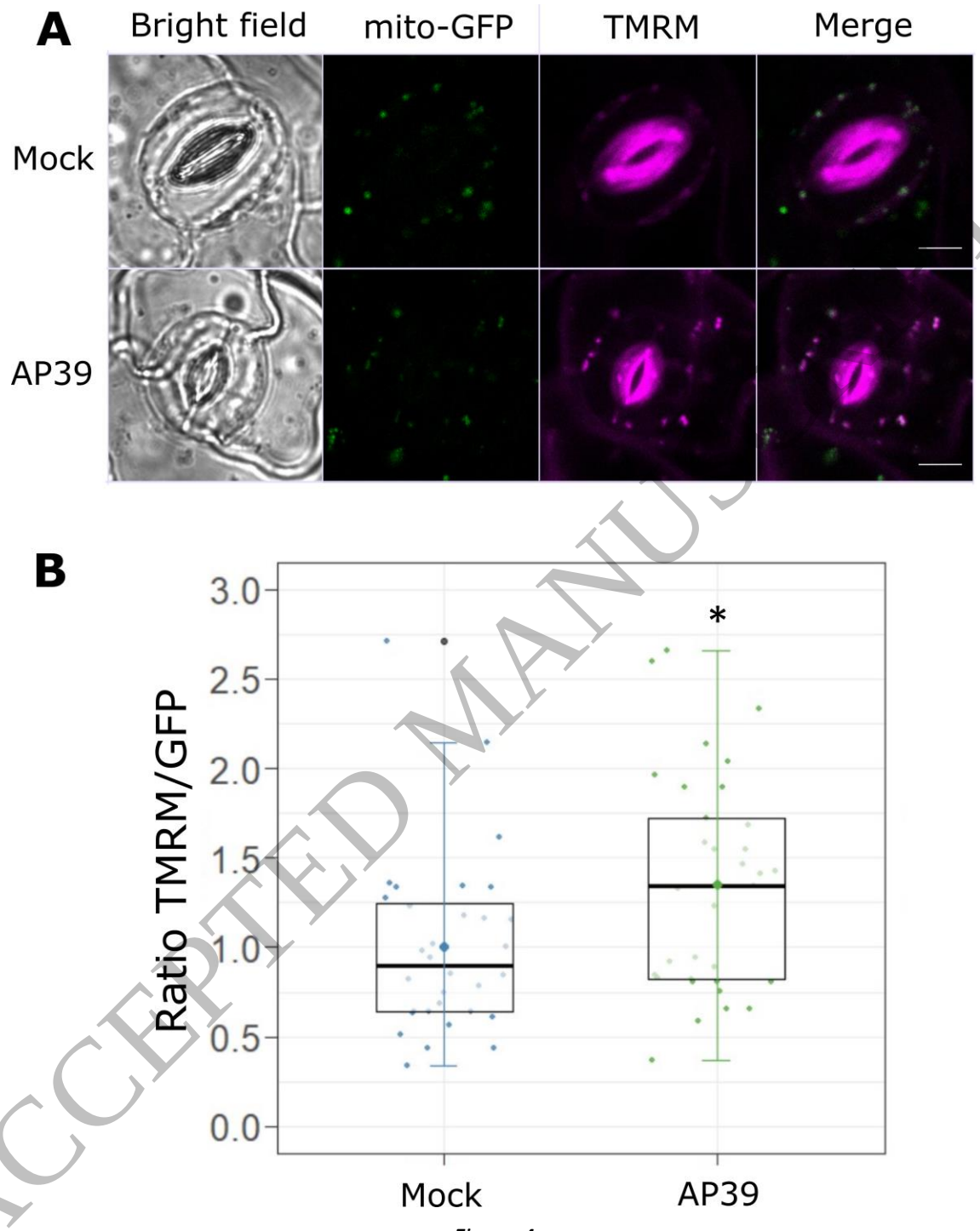

Figure 4
150x187 mm (3.2 x DPI)

1

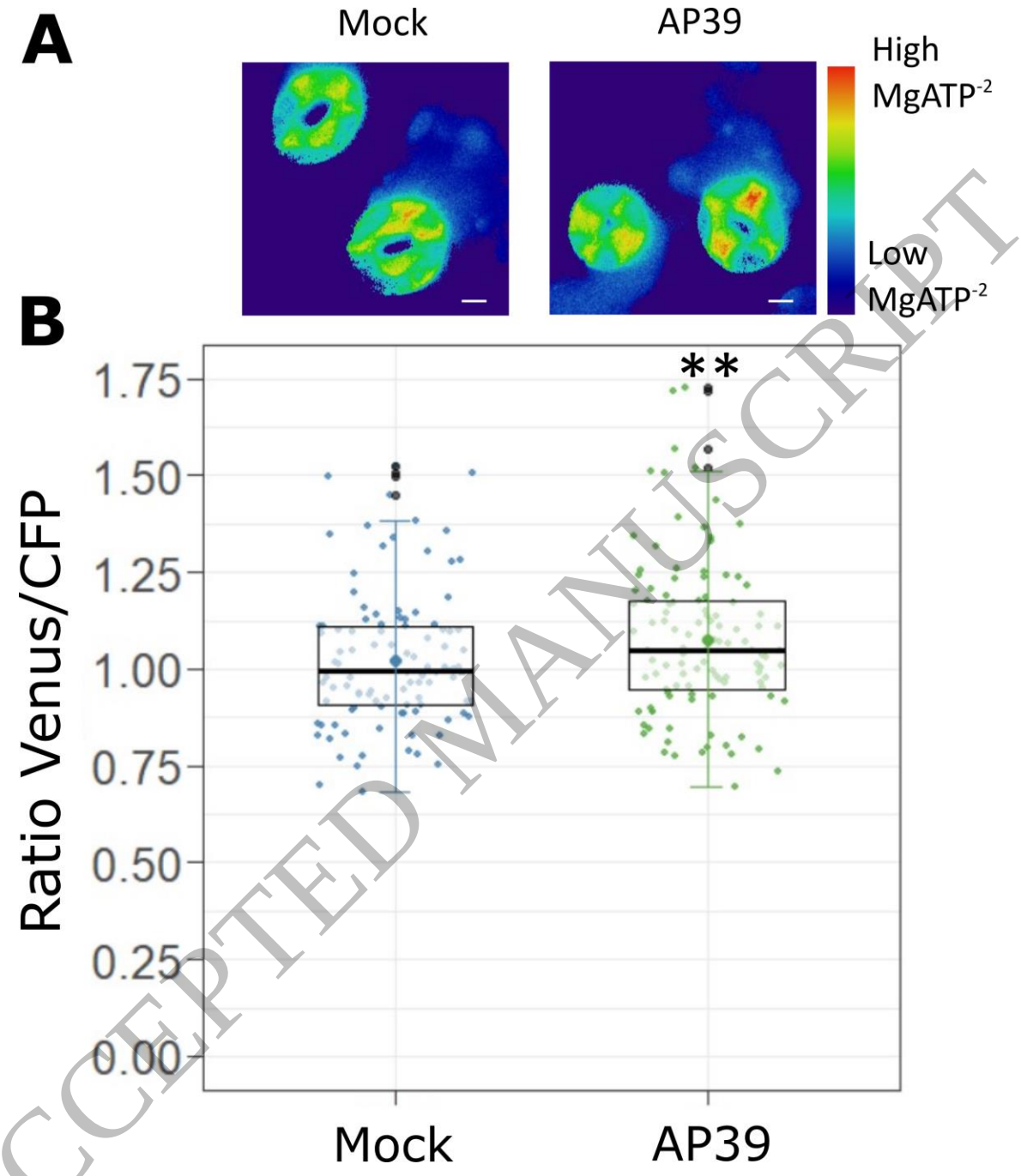

Figure 5
150x178 mm (3.2 x DPI)

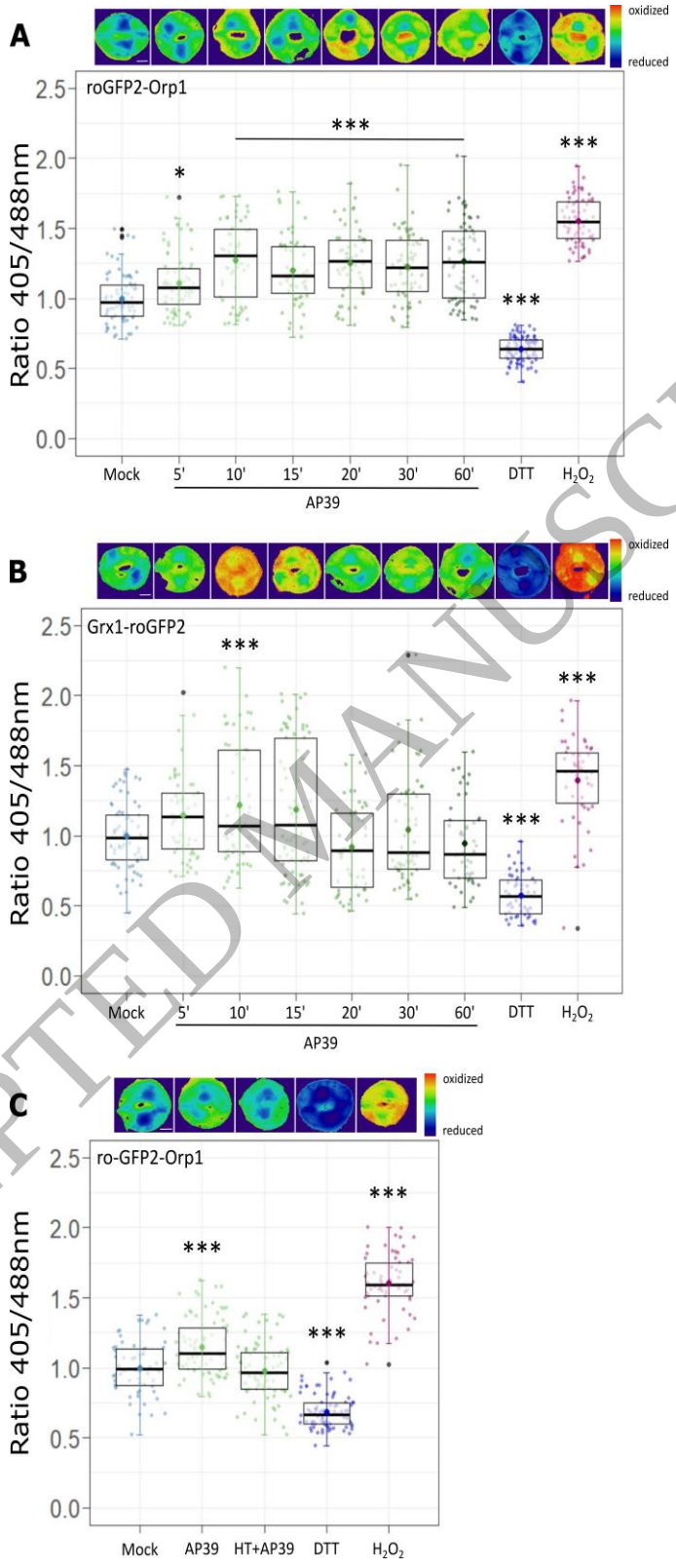

Figure 6
120x247 mm (3.2 x DPI)

1

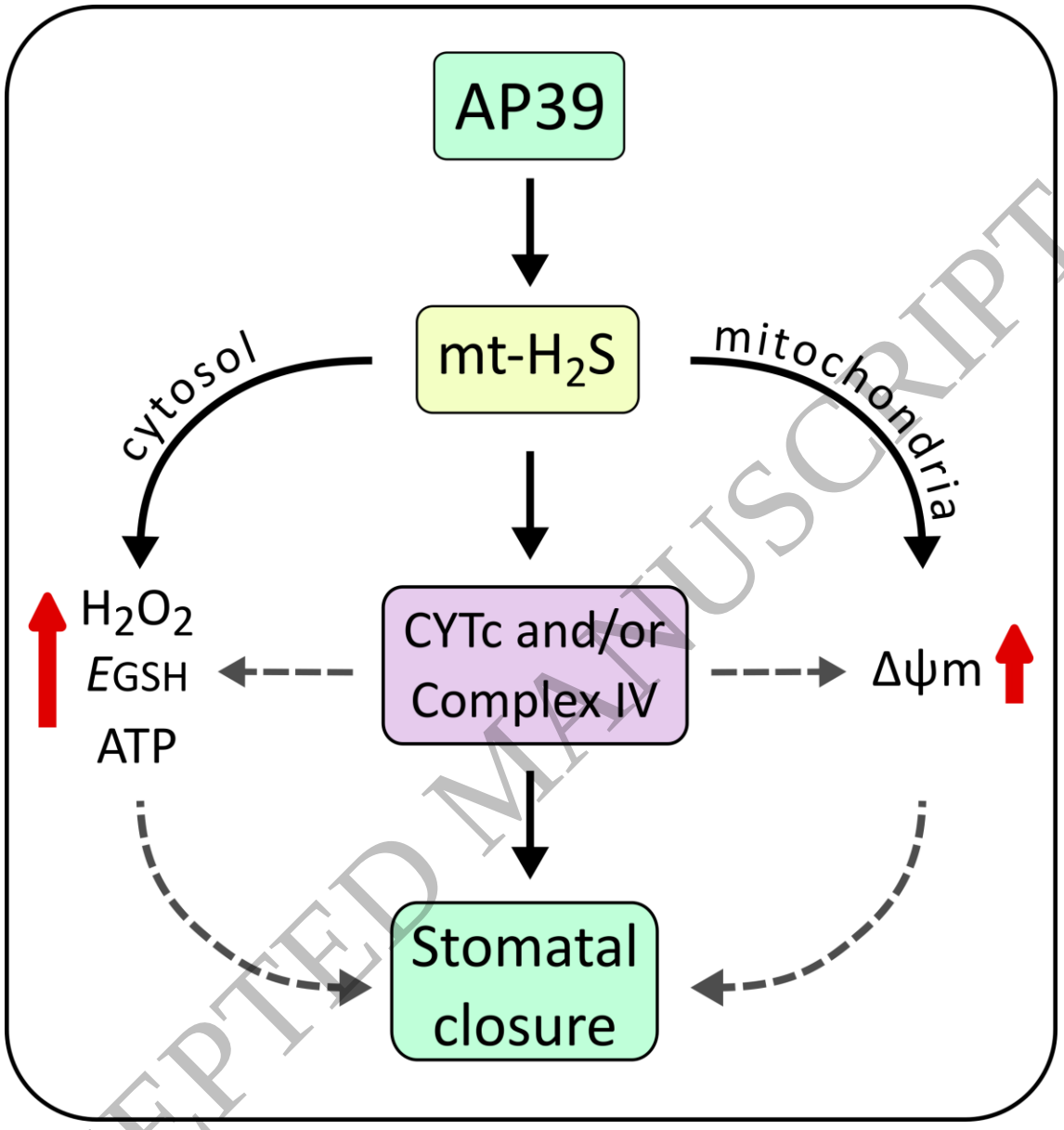

Figure 7
150x159 mm (3.2 x DPI)